IVYSPRING INTERNATIONAL PUBLISHER

Theranostics

2017; 7(10): 2565-2574. doi: 10.7150/thno.19900

Research Paper

Targeting Activated Platelets: A Unique and Potentially Universal Approach for Cancer Imaging

May Lin Yap[1, 2*], James D McFadyen[1, 3, 4*], Xiaowei Wang[1, 3*], Nicholas A Zia[5, 6], Jan David Hohmann[1], Melanie Ziegler[1], Yu Yao[1], Alan Pham[7], Matthew Harris[5], Paul S Donnelly[6], P Mark Hogarth[2, 8, 9], Geoffrey A Pietersz[1, 2, 8, 9], Bock Lim[1‡], Karlheinz Peter[1, 3, 9‡]✉

1. Baker Heart and Diabetes Institute, Melbourne, 3004, Australia
2. Department of Pathology, The University of Melbourne, Melbourne, 3010, Australia
3. Department of Medicine, Monash University, Melbourne, 3800, Australia
4. Department of Hematology, The Alfred Hospital, Melbourne, 3004, Australia
5. Clarity Pharmaceuticals, Sydney, 2014, Australia
6. School of Chemistry and Bio21 Molecular Science and Biotechnology Institute, The University of Melbourne, 3010, Melbourne, Australia
7. Department of Anatomical Pathology, The Alfred Hospital, Melbourne, 3004, Australia
8. Burnet Institute, Melbourne, 3004, Australia
9. Department of Immunology, Monash University, Melbourne, 3800, Australia

* equally contributing first authorship

‡ equally contributing senior authorship

✉ Corresponding author: Karlheinz.Peter@baker.edu.au

Received: 2017.03.03; Accepted: 2017.04.26; Published: 2017.06.25

Abstract

Rationale The early detection of primary tumours and metastatic disease is vital for successful therapy and is contingent upon highly specific molecular markers and sensitive, non-invasive imaging techniques. We hypothesized that the accumulation of activated platelets within tumours is a general phenomenon and thus represents a novel means for the molecular imaging of cancer. Here we investigate a unique single chain antibody (scFv), which specifically targets activated platelets, as a novel biotechnological tool for molecular imaging of cancer.

Methods The scFv$_{GPIIb/IIIa}$, which binds specifically to the activated form of the platelet integrin receptor GPIIb/IIIa present on activated platelets, was conjugated to either Cy7, ^{64}Cu or ultrasound-enhancing microbubbles. Using the Cy7 labelled scFv$_{GPIIb/IIIa}$, fluorescence imaging was performed in mice bearing four different human tumour xenograft models; SKBr3, MDA-MB-231, Ramos and HT-1080 cells. Molecular imaging via PET and ultrasound was performed using the scFv$_{GPIIb/IIIa}$-^{64}Cu and scFv$_{GPIIb/IIIa}$-microbubbles, respectively, to further confirm specific targeting of scFv$_{GPIIb/IIIa}$ to activated platelets in the tumour stroma.

Results Using scFv$_{GPIIb/IIIa}$ we successfully showed specific targeting of activated platelets within the microenvironment of human tumour xenografts models via three different molecular imaging modalities. The presence of platelets within the tumour microenvironment, and as such their relevance as a molecular target epitope in cancer was further confirmed via immunofluorescence of human tumour sections of various cancer types, thus validating the translational importance of our novel approach to human disease.

Conclusion Our study provides proof of concept for imaging and localization of tumours by molecular targeting activated platelets. We illustrate the utility of a unique scFv as a versatile biotechnological tool which can be conjugated to various contrast agents for molecular imaging of cancer using three different imaging modalities. These findings warrant further development of this activated platelet specific scFv$_{GPIIb/IIIa}$, potentially as a universal marker for cancer diagnosis and ultimately for drug delivery in an innovative theranostic approach.

Key words: Cancer, Activated Platelets, PET, Fluorescence Imaging, Ultrasound.

Introduction

The early detection of primary tumours and early metastatic disease is critical for the successful implementation of remission induction therapies[1]. Given the current, often limited success of cancer treatment and the expectation that the global burden of cancer will increase[2], the development of new methods to detect the early stages of primary or metastatic cancer are needed and highly sought-after. Particularly, the development of non-invasive imaging techniques targeting a universal molecular marker of tumours would represent an eminent diagnostic tool.

The connection between cancer and platelets has been postulated for over 100 years, and it is now well appreciated that a significant proportion of patients with cancer demonstrate an elevated platelet count, and is associated with an adverse prognosis[3,4]. Tumour cells have been demonstrated to induce platelet aggregation, a process known as tumour cell-induced platelet aggregation (TCIPA)[5,6]. Mechanistically, tumour cells are known to release platelet agonists such as thromboxane-A_2 (TXA_2), adenosine diphosphate (ADP) and matrix metalloproteinase-2 (MMP-2)[7-9]. In addition, platelet receptors such as GPIb, GPIIb/IIIa and P-selectin have also been shown to directly interact with cancer cells, promoting platelet activation and aggregation[10–13]. GPIIb/IIIa, the most abundant platelet receptor, is a platelet specific integrin, with approximately 50,000-80,000 copies per platelet[14] that upon platelet activation, undergoes a conformational change from the resting, low affinity state towards a high affinity state, thus exposing neoepitopes and the ligand binding domain[15]. Therefore, postulating the presence of activated platelets in the tumour microenvironment, we hypothesized that the activated conformation of the platelet GPIIb/IIIa represents a novel marker for detection and imaging of cancer.

Here, using a single-chain antibody (scFv) which specifically targets the active conformation of GPIIb/IIIa of both human and mouse activated platelets[16–18], we demonstrate for the first time the ability to image tumours *in vivo* by targeting activated platelets using a GPIIb/IIIa scFv. The scFv was conjugated to three different contrast agents; Cy7 for fluorescence imaging, ^{64}Cu for PET imaging and microbubbles for ultrasound imaging. This novel approach provides holds promise as a universal and flexible diagnostic method for the detection and imaging of cancer.

Results

Platelets are abundant within a broad range of primary human tumours

To investigate the presence of platelets within the three most common types of human tumours, sections of breast, bowel and lung adenocarcinoma from patients were stained for platelets. CD41, the GPIIb subunit of the GPIIb/IIIa heterodimer is both platelet specific and forms part of the most abundant platelet receptor, GPIIb/IIIa, and was therefore used as a platelet marker in tumours[19,20]. Human tumour sections were stained with a CD41 antibody and imaged with confocal immunofluorescence microscopy. Strikingly, all of these human tumours displayed an abundance of platelets (Fig 1A-C). In contrast, sections of healthy human breast, bowel and lung not involved in tumour displayed no detectable CD41 staining (Fig 1D-F).

We then aimed to determine the presence of platelets in four distinct human tumour xenografts from mice. Utilizing two models of breast cancer (SKBr3 and MDA-MB-231), a model of fibrosarcoma (HT-1080) and Burkitt's lymphoma (Ramos), tumour sections were stained for platelets with CD41 antibody. Consistent with our histology from patient tumour sections, all human xenograft subtypes displayed abundant platelet staining within the tumour tissue (Fig 2A-D). As a negative control, healthy muscle adjacent to tumours displayed no CD41 staining (Fig 2E). Parallel flow cytometry analysis of MDA-MB-231 and Ramos tumours demonstrated that 17.67±0.88 % (n=3 vs. n=5, $p<0.001$) and 14.00±2.34 % (n=5 vs. n=5, $p<0.001$) of all cells respectively, within these tumours are CD41 positive, thus confirming the abundance of platelets within primary tumours (Fig 2F). In contrast, healthy muscle taken from these mice contained few platelets with less than 1% of all cells being CD41 positive. Taken together, these findings show that platelets are present in large numbers within a broad range of human and mouse xenograft tumours.

Having demonstrated that tumour sections exhibit an abundance of platelets within the tumour microenvironment, we sought to examine if tumour cells can directly cause platelet activation. The human cancer cell line SKBr3, were incubated with washed human platelets for 2 hours. Platelet activation was then assessed using confocal immunofluorescence microscopy by the binding of three distinct activation specific antibodies; PAC-1 and $scFv_{GPIIb/IIIa}$–GFP which binds the activated conformation of GPIIb/IIIa or P-selectin, a marker of platelet alpha granule exocytosis. Consistent with the ability of tumour cells to directly activate platelets, SKBr3 tumour cells

directly bound platelets and resulted in platelet activation as shown by increased PAC-1 and $scFv_{GPIIb/IIIa}$-GFP binding and P-selectin expression (Fig 2G-I). These results highlight the ability of tumour cells to directly activate platelets in addition to providing *in vitro* validation of our $scFv_{GPIIb/IIIa}$ to recognize tumour associated activated platelets.

Specific tumour localization of $scFv_{GPIIb/IIIa}$-Cy7 in SKBr3, Ramos, HT-1080 and MDA-MB-231 xenografts via fluorescence imaging

Given the demonstrated abundance of platelets in various tumour tissues and the described ability of tumour cells to activate platelets[6], we postulated that activated platelets could serve as a general molecular marker for cancer imaging. Therefore, scFvs specific for activated platelets ($scFv_{GPIIb/IIIa}$) and a mutant non-targeting scFv ($scFv_{mut}$) were conjugated to Cy7 and intravenously injected into mice bearing SKBr3, Ramos, HT-1080 or MDA-MB-231 xenografts prior to undergoing Fluorescence Emission Computed Tomography (FLECT) imaging. In accordance with our *in vitro* data, all four xenograft models demonstrated significant fluorescence signal in the area of tumour in mice injected with $scFv_{GPIIb/IIIa}$-Cy7 tracer compared to control $scFv_{mut}$-Cy7 tracer, represented by images of SKBr3 bearing xenograft mice in Fig 3A. The tumour to muscle signal ratio of the SKBr3 tumour bearing mice injected with the $scFv_{GPIIb/IIIa}$-Cy7 and $scFv_{mut}$-Cy7 tracer was 2.89±0.32 and 1.26±0.12, respectively (n=11 vs. n=9, $p<0.001$) (Fig 3B). Similarly, in Ramos and HT-1080 tumour bearing mice, the tumour to muscle ratio was 3.05±0.53 vs. 1.07±0.11 (n=7 vs. n=6, $p<0.01$) and 2.03±0.19 vs. 0.67±0.13 (n=6 vs. n=6, $p<0.001$), respectively in mice given the $scFv_{GPIIb/IIIa}$-Cy7 vs. $scFv_{mut}$-Cy7 tracer (Fig 3B). In mice injected with the triple-negative breast cancer line, MDA-MB-231, the tumour to muscle ratio was 2.48±0.28 in mice injected with $scFv_{GPIIb/IIIa}$-Cy7 and 1.41±0.21 in mice injected with the control tracer (n=7 vs. n=7, $p<0.01$) (Fig 3B). Complementary imaging using a 2D *in vivo* imaging system (IVIS) demonstrated that the tumour xenografts, *in vivo* and *ex vivo,* display increased NIR signal in mice injected with $scFv_{GPIIb/IIIa}$-Cy7, but not $scFv_{mut}$-Cy7, thus confirming the specific binding of $scFv_{GPIIb/IIIa}$-Cy7 tracer to activated platelets present amongst the tumour microenvironment (Fig 3C and 3D).

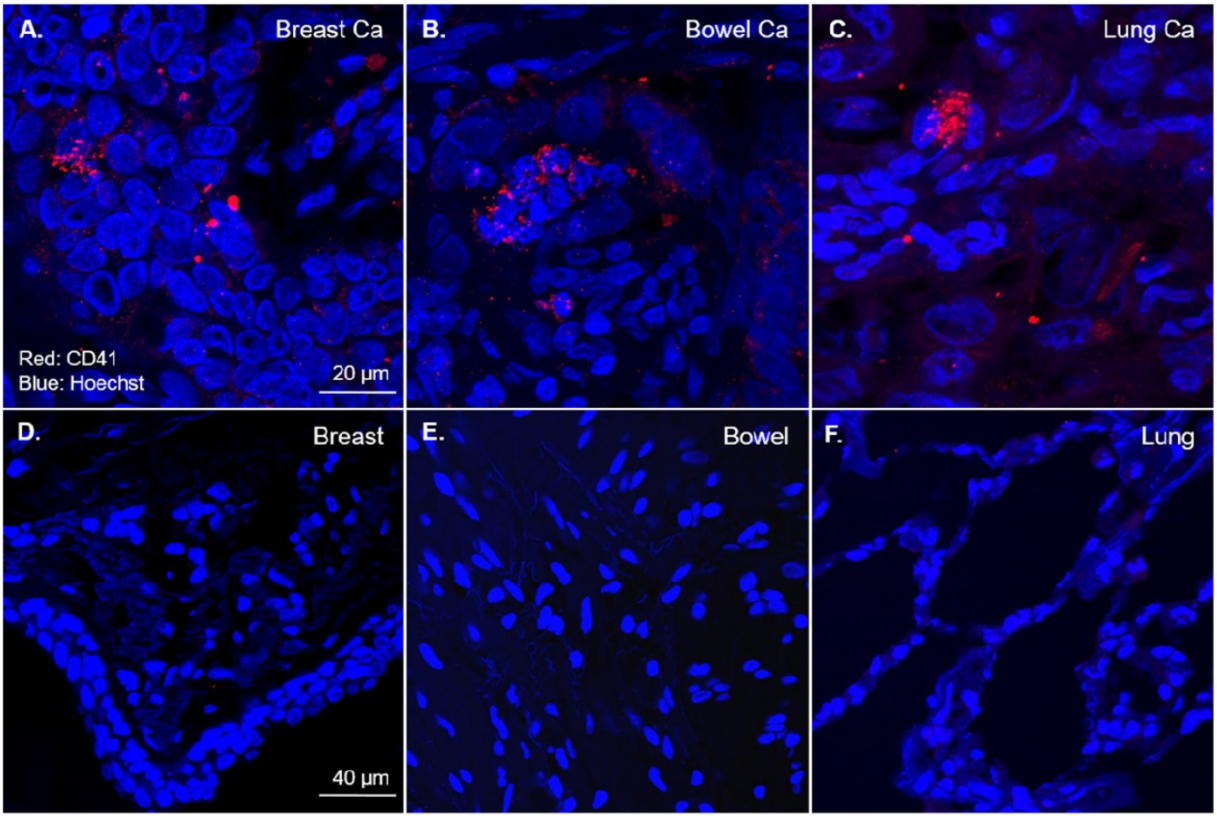

Figure 1. Platelets are abundant in common human tumours but not in healthy tissues. Formalin fixed sections from primary human adenocarcimonas and healthy human tissues underwent immunofluorescence for platelets (red) and nuclei (blue) with an anti-CD41 antibody and counterstained with Hoechst® nucleic acid stain. Representative 60x magnification confocal fluorescence microscopy images demonstrating the presence of platelets within primary human breast (n=3), bowel (n=3) and lung (n=3) adenocarcinomas **(A-C)**. Representative 60x magnification confocal fluorescence microscopy images of healthy breast (n=2), bowel (n=2) and lung (n=2) tissues displaying no CD41 staining **(D-F)**.

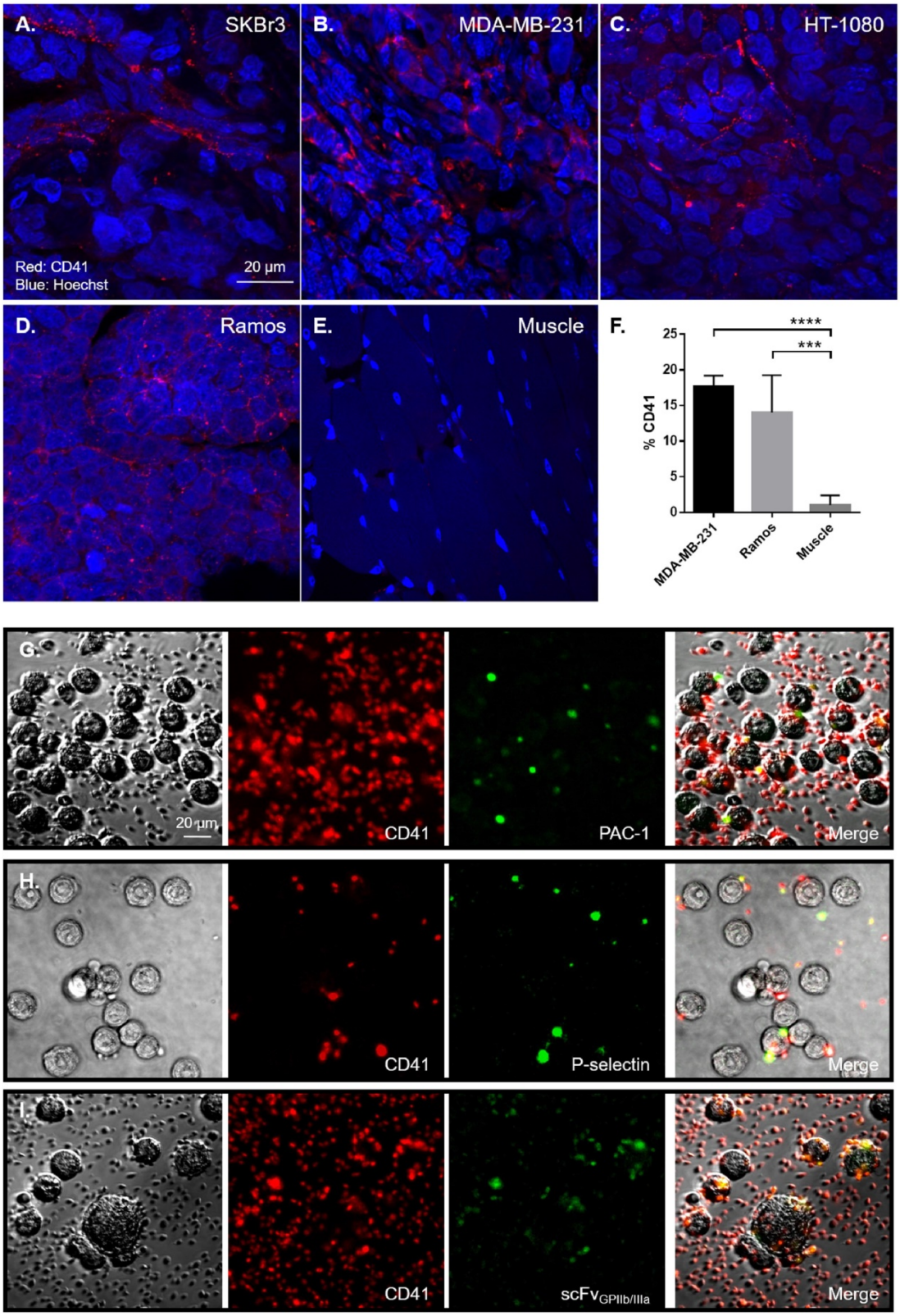

Figure 2. Platelets are abundant in human xenografts and are activated by tumour cells. Formalin fixed sections from human xenografts underwent immunofluorescence for platelets (red) and nuclei (blue) with an anti-CD41 antibody and counterstained with Hoechst® nucleic acid stain. Representative 60x magnification confocal fluorescence microscopy images of mice bearing SKBr3 (n=4), MDA-MB-231 (n=4), HT-1080 (n=4) and Ramos (n=4) tumour xenografts sections shows CD41 positive (red) staining **(A-D)**, demonstrating that similar to human tumours, platelets are present within distinct mouse xenograft tumour tissues, compared to healthy muscles **(E)**. Quantitative analysis of the number of platelets within MDA-MB-231 (n=3) and Ramos (n=5) tumours was performed by CD41 staining in flow cytometry, compared to healthy muscles (n=5) **(F)**. To demonstrate the ability of tumour cells to directly activate platelets, SKBr3 cells were incubated with human platelets for 2 hours *in vitro*. Platelets were then stained with a CD41 antibody (red) and the platelet activation markers PAC-1 binding (green) **(G)**, P-selectin expression (green) **(H)** and $scFv_{GPIIb/IIIa}$ binding (green) **(I)** was determined, demonstrating the presence of activated platelets on the tumour cells. Statistical analysis was performed using one way ANOVA and statistical significance was assigned for p values <0.001, represented by ***.

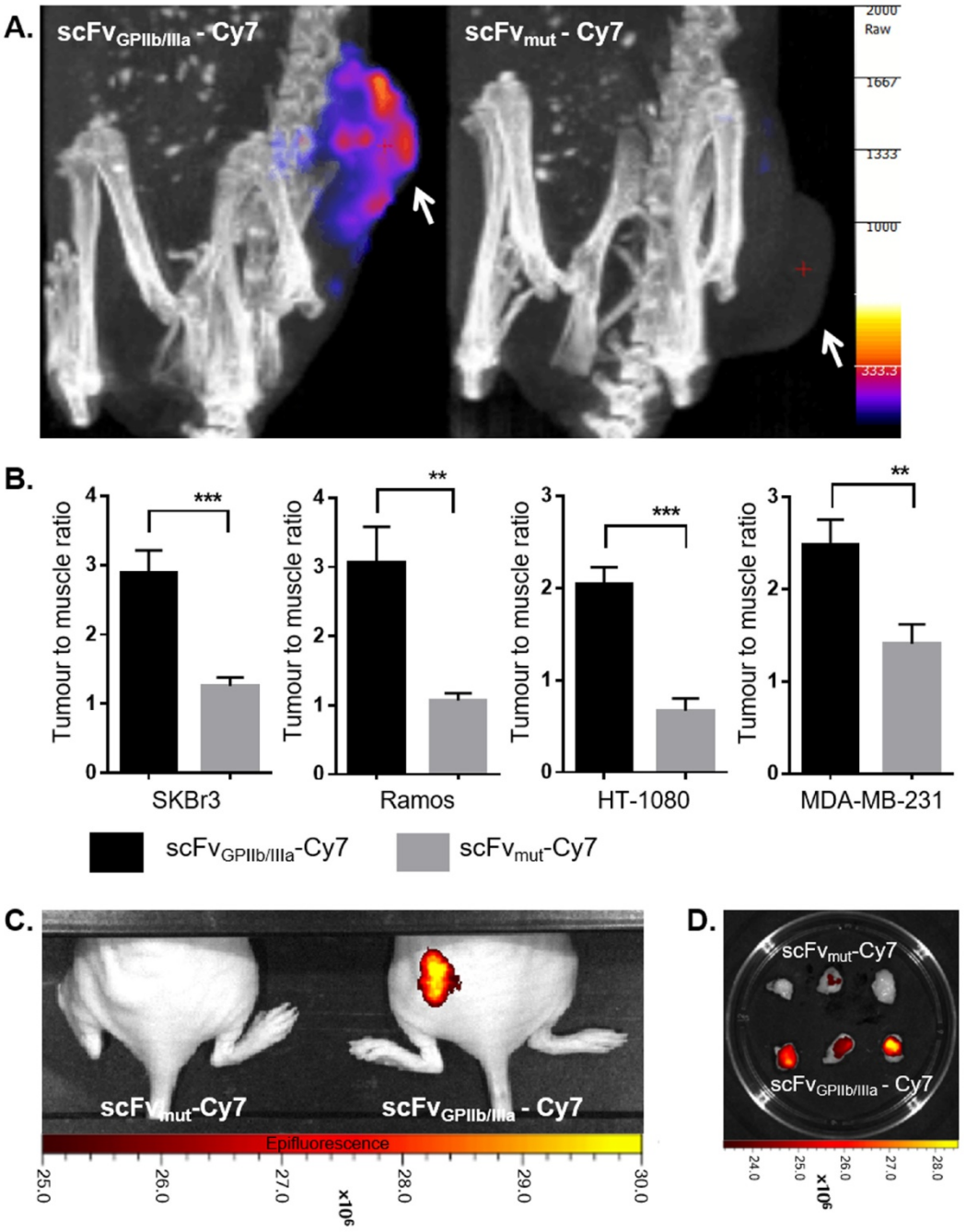

Figure 3. Specific tumour localization of ScFv$_{targ}$-Cy7 via fluorescence imaging. FLECT imaging of SKBr3 tumour-bearing BALB/c nude mice at 20 hours post injection of scFv$_{GPIIb/IIIa}$-Cy7 or scFv$_{mut}$-Cy7, with areas of tumours indicated by a white arrow (**A**). Quantification of mean fluorescence intensity of mice injected with scFv$_{GPIIb/IIIa}$-Cy7 and scFv$_{mut}$-Cy7 was presented as tumour to muscle ratio for SKBr3 xenografts; (n=11) and (n=9), Ramos Xenografts; (n=7) and (n=6), HT-1080 Xenografts; (n=6) and (n=6) and MDA-MB-231 xenografts; (n=7) and (n=7) (**B**). Mice were also imaged with a 2D IVIS scanner 20 hours following injection of tracer (**C**). Ramos tumour sections of mice injected with scFv$_{GPIIb/IIIa}$-Cy7 or ScFv$_{mut}$-Cy7 were excised and imaged with IVIS (**D**). Statistical analysis was performed using unpaired Student's T test and statistical significance was assigned for p values <0.01 and <0.001, and represented by ** and ***, respectively.

Specific tumour targeting of scFv$_{GPIIb/IIIa}$-^{64}Cu SKBr3 xenograft via PET/CT

Having demonstrated the utility of imaging activated platelets across a range of tumours using fluorescence imaging, we then assessed the imaging of activated platelets in tumours using PET. Since breast cancer is one of the most common tumour types seen in the clinic and as such, novel imaging approaches towards early and sensitive detection of these tumours are of particular translational relevance, the SKBr3 xenograft model was evaluated in PET/CT imaging. The scFvs were conjugated to a bifunctional sarcophagine chelator, MeCOSar and labelled with copper-64 to produce scFv$_{GPIIb/IIIa}$-^{64}Cu and scFv$_{mut}$-^{64}Cu[21,22]. The radiotracers were injected

intravenously to SKBr3 xenografts bearing mice and PET scans acquired 2 hours post-injection. We observed increased radiotracer uptake in the tumour region of mice injected with $scFv_{GPIIb/IIIa}$-^{64}Cu compared to the control group as shown in Fig 4A. Radiotracer uptake was determined by gamma counting and presented as percentage injected dose per gram (% ID/g) of tumour to muscle ratio. As we have previously shown that $scFv_{GPIIb/IIIa}$-^{64}Cu was cleared from the circulation within 30 min to 1 hour[21], in this study the tumour to muscle ratio was calculated to demonstrate a means of differentiating the retention of $scFv_{GPIIb/IIIa}$-^{64}Cu in the tumour versus a healthy tissue. The % ID/g tumour to muscle ratio was 5.94±1.19 in mice injected with $scFv_{GPIIb/IIIa}$-^{64}Cu and 2.33±0.33 in mice injected with $scFv_{mut}$-^{64}Cu (n=7 vs. n=5, p<0.05), shown in Fig 4B.

Specific tumour targeting of $scFv_{GPIIb/IIIa}$-MB in SKBr3 xenograft via ultrasound imaging

To examine the utility of our platelet-targeted approach using ultrasound, both $scFv_{GPIIb/IIIa}$ and $scFv_{mut}$ were biotinylated in order to enable direct conjugation with streptavidin-coated microbubbles (MBs) to obtain $scFv_{GPIIb/IIIa}$-MBs and $scFv_{mut}$-MBs respectively[23]. Either $scFv_{GPIIb/IIIa}$-MBs or $scFv_{mut}$-MBs were intravenously injected and images recorded at baseline (before injection), 5 and 10 min post injection (Fig 4C). In accordance with our FLECT and PET imaging studies, we observed increased contrast intensity of mice injected with $scFv_{GPIIb/IIIa}$-MBs compared to the control group. At 5 min, the mean increase in contrast intensity was 57.85±6.50 in mice injected with $scFv_{GPIIb/IIIa}$-MBs as compared to 9.48±2.04 in mice injected with $scFv_{mut}$-MBs (n=4 vs. n=3, p<0.001). After 10 min, the mean increase in contrast intensity was 55.16±11.58 in mice injected with $scFv_{GPIIb/IIIa}$-MBs and 5.67±0.14 in mice injected with $scFv_{mut}$-MBs (n=4 vs. n=3, p<0.001) (Fig 4D). These findings demonstrate that activated platelets can be used to specifically detect a broad range of tumours *in vivo* using distinct molecular imaging modalities.

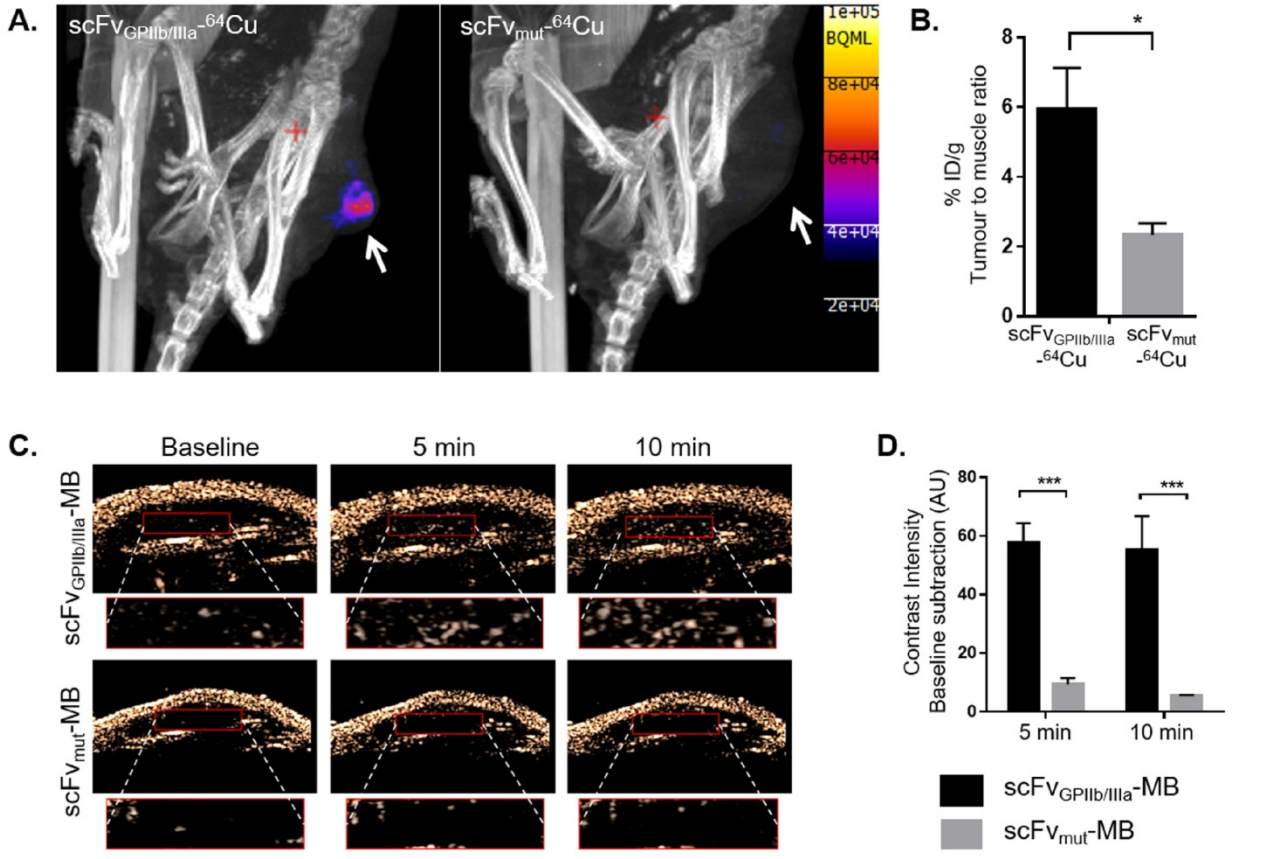

Figure 4. Specific localization of $scFv_{GPIIb/IIIa}$ in SKBr3 xenograft via PET/CT and ultrasound imaging. Nano PET/CT imaging of SKBr3 tumour bearing BALB/c nude mice at 2 hour post injection of $scFv_{GPIIb/IIIa}$-^{64}Cu (n=7) or $scFv_{mut}$-^{64}Cu (n=5) (**A**) with areas of tumours indicated by a white arrow. Quantification of radiation intensity was presented as percentage injected dose/gram (% ID/g) of tumour normalised to muscle signals (**B**). Ultrasound imaging of SKBr3 tumour bearing BALB/c nude mice at baseline, 5 and 10 min post injection of $scFv_{GPIIb/IIIa}$-MB (n=4) or $scFv_{mut}$-MB (n=3). The bottom panel of each image indicates a zoomed-in magnification of the tumour (red box) and the contrast intensity visualization within this tumour region (**C**). Quantification was presented as contrast intensity baseline subtraction (AU) (**D**). Statistical analysis was performed using unpaired Student's T test and statistical significance was assigned for p values <0.05 and <0.001, and represented by * and ***, respectively.

Discussion

We demonstrate that activated platelets can be targeted to specifically diagnose and image a broad range of tumours *in vivo*. The ability of tumour cells to activate platelets, the demonstrated abundance of platelets in the tumour microenvironment and high numbers of GPIIb/IIIa on platelets[5,14], makes the platelet receptor GPIIb/IIIa an ideal target for molecular imaging of tumours.

The central element of our study is the ability to target and image activated platelets as a general component of the tumour microenvironment, thereby defining a novel non-invasive technique to diagnose and localize tumours *in vivo*. In addition, we demonstrate the feasibility of Cy7, ^{64}Cu and microbubbles as conjugates to the $scFv_{GPIIb/IIIa}$ for imaging tumours *in vivo*. The ability to use the recombinant single-chain antibody $scFv_{GPIIb/IIIa}$, which specifically binds to activated platelets have been characterized extensively in previous *in vivo* studies[24–27], and thus provides a solid foundation to define activated platelets as a marker of the tumour microenvironment. Furthermore, our finding provides the basis for two potentially far-reaching perspectives: Firstly, irrespective of the coupling approach, the specificity and sensitivity of the $scFv_{GPIIb/IIIa}$ allowed strong targeting to activated platelets and thus represents a unique foundation of this molecular target as a unique approach for tumour imaging. Clinically, imaging of activated platelets in cancer holds promise as an auxiliary imaging strategy to allow the accurate delineation of the anatomic distribution of tumours. Although further studies are required to investigate our novel imaging approach in additional tumour types and in detecting metastatic lesions, this study provides a proof of concept that activated platelets can act as a specific molecular marker for a large range of tumours. Secondly, the $scFv_{GPIIb/IIIa}$ provides the foundation for investigating the potential of activated platelet-specific scFv targeted drug delivery as means to enhance the efficacy[28–30], whilst minimizing the systemic toxicity of chemotherapy.

Materials and Methods

Study Approval

All animal studies were conducted in strict accordance with protocols approved by the Alfred Medical Research Education Precinct Animal Ethics Committee and the Monash University Animal Ethics Committee. Human tumour sections were obtained from biopsy specimens from patients with histologically confirmed breast, bowel or lung adenocarcinoma with approval by the Alfred Medical Research Education Precinct, Human Research Ethics Committee (Project number 88/16).

Generation of scFv-Biotin

The generation of biotinylated $scFv_{GPIIb/IIIa}$ and $scFv_{mut}$ has been described previously[23]. Both scFvs were sub-cloned into the AviTag™ containing pAC6 vector system, the DNA was then transformed into electrocompetent cell *E. coli* EVB101 (Avidity LLC) by electroporation. *In vivo* biotinylation was performed according to the manufacturer's instruction producing the attachment of one biotin molecule on every scFv.

Generation of scFv-LPETG

Using polymerase chain reaction (PCR) reaction, the LPETG tag as a sortase recognition sequence was introduced to the C-terminal end of the scFv. The entire scFv was then subcloned into a pSectag 2A vector (Invitrogen) for expression in human embryonic kidney cells (Invitrogen)[29].

Conjugation of scFvs to Cy7

The $scFv_{GPIIb/IIIa}$ and $scFv_{mut}$ constructed with a LPETG tag on the C-terminus were labelled with Cy7 using a Sortase A enzyme-based protocol[31]. Briefly, the Sortase A enzymatic reaction enables the conjugation of the LPETG with a glycine residue on the N-terminal of a cyclooctyne compound, bicyclo-[6.1.0]-non-4-yne (BCN) to form scFv-BCN. The resultant scFv-BCN was further conjugated to an azide-NIR dye (azide-Cyanine 7 dye) via copper-free click reaction to generate the FLECT tracer. Excess free dye was dialysed in PBS and the purified scFv-Cy7 was analyzed on a SDS-PAGE gel and NIR signal from the band of interest was confirmed using the Odyssey Imager.

^{64}Cu Production and scFv Radiolabeling

$^{64}CuCl_2$ produced by the $^{64}Ni(p,n)^{64}Cu$ reaction was obtained from the Austin Health Centre for PET. The solution was provided with a radionuclidic purity, tested using gamma ray spectrometry of >99% and a radiochemical purity, tested using HPLC of >95%.

The scFv used for PET/CT imaging were conjugated to a sarcophagine chelator, MeCOSar (Clarity Pharmaceuticals)[21,22]. For radiolabeling: to a mixture of scFv-MeCOSar (100 µg, in PBS), was $^{64}CuCl_2$ (50 MBq) added at room temperature. After 30 min, diethylenetriaminepentaacetic acid (10 µL, 10 mM) was added to the mixture and incubated for a further 5 min at room temperature. Samples were washed twice with PBS in spin columns (Millipore, cutoff 10,000 MWCO) and resuspended in PBS at a

final concentration of 0.2 mg/mL to produce $scFv_{GPIIb/IIIa}$-^{64}Cu or $scFv_{mut}$-^{64}Cu.

Conjugation of scFv-Biotin to Microbubbles

Biotinlyated scFvs (4 µg) were directly added to a vial of target-ready microbubbles MBs (VisualSonics, Inc) and incubated at room temperature for 20 min[23]. The scFv-MBs were placed on ice and used within 6 hours of conjugation.

Cancer Cell Lines

Human cancer cell lines SKBr3, MDA-MB-231, Ramos and HT-1080 were cultured in RPMI media (GIBCO® #21870) supplemented with 10% (v/v) FBS (Invitrogen), 100 U/ml penicillin, and 0.1 mg/ml streptomycin at 37°C in a 5% CO_2 humidified atmosphere.

Preparation of Human Washed Platelets

Fresh blood was drawn from informed healthy volunteers who had not taken anti-platelet drugs at least two weeks prior to venesection. Blood was collected into acid citrate dextrose (ACD; 85 mM sodium citrate, 72.9 mM citric acid, 110 mM D-glucose, 70 mM theophylline) (at a ratio of ACD:blood of 1:6) and supplemented with apyrase 0.005 U/mL and enoxaparin 20 U/mL. Whole blood was centrifuged at 200 g for 10 min. Platelet rich plasma (PRP) was obtained and then centrifuged at 1700g for 7 min. The platelet poor plasma (PPP) was removed and platelets resuspended in platelet washing buffer (pH 6.5; 4.3 mM K_2HPO_4; 4.3 mM Na_2HPO_4; 24.3 mM NaH_2PO_4; NaCl 0.113 M; 5.5 mM D-glucose; 10 mM theophylline) supplemented with enoxaparin (20 U/mL), apyrase (0.01U/mL) and 0.5% BSA. Finally, washed platelets were resuspended in Tyrode's buffer (pH 7.2-7.4; 12 mM $NaHCO_3$; Hepes 10 mM; NaCl 0.137 M; KCL 27 mM; D-glucose 55 mM) containing 1 mM CaCl and apyrase 0.02 U/mL.

Tumour Xenograft Model

5-6 weeks old female BALB/c nude mice were purchased from the Animal Resources Centre, Canningvale. To establish tumour xenografts, mice were injected subcutaneously with exponentially growing SKBr3, MDA-MB-231, Ramos or HT-1080 cells (2.0×10^6 cells per mouse) in 0.3 ml of matrigel (BD Biosciences #356234) into the left flank region. Tumours were left to grow and measured daily until reaching a diameter of approximately 4 mm, which usually appears 2-3 weeks post xenograft cell injection.

In vivo Fluorescence Tomography Imaging of Tumour

Animals were injected intravenously with 20 µg $scFv_{GPIIb/IIIa}$-Cy7 or $scFv_{mut}$-Cy7 and tracer was allowed to circulate for 20 hours. Animals were anesthetized with ketamine (50 mg/kg; Parnell Laboratories) and xylazine (10 mg/kg; Troy Laboratories) and placed in the FLECT scanner supplied with continuous O_2 and 2% isofluorane. Fluorescence imaging was performed using the Trifoil InSyTe FLECT® imager using the following filters (Excitation - 730 and emission – 803) at 500ms at each frame. A CT scan was then performed using a Trifoil microCT *in vivo* Preclinical Imager using the following settings (X-ray voltage = 55 kVp, Exposure time = 1100 ms and Pitch= 1). A total projection of 180 projects over 360° of rotation was acquired. Projected data were rebinned by 1:4 and reconstructed using Butterworth filter. The FLECT and CT scan images were then fused and co-registered using the InVivoScope version 2.00-analysis software. For fluorescence quantification, a region-of-interest (ROI) was drawn around the area of tumour and mean fluorescence intensity (MFI) was quantified using the InVivoScope version 2.00 analysis software.

IVIS Imaging

Following FLECT imaging, 2D fluorescence imaging of mice was performed using the IVIS Lumina Series II Imaging System (Perkin Elmer) using the following settings (Filter Passband = Excitation 710-760 nm, Emission 810-875 nm). Fluorescence intensity of tumours and other organs was calculated using the Living Image software v4.5.1 (Perkin Elmer) and presented as Average Radiant Efficiency [p/s/cm²/sr] / [µW/cm²].

In vivo PET Imaging

Animals were injected intravenously with 20 µg $scFv_{GPIIb/IIIa}$-^{64}Cu or $scFv_{mut}$-^{64}Cu. Tracer was allowed to circulate for two hours. Animals were anesthetized with ketamine (50 mg/kg; Parnell Laboratories) and xylazine (10 mg/kg; Troy Laboratories) and placed in the PET/CT scanner supplied with continuous O_2 and 2% isofluorane. PET/CT imaging was performed using a NanoPET/CT *in vivo* Preclinical Imager (Mediso) with a 30 min PET acquisition time, and coincidence mode of 1:3. This was followed by a CT scan with the following parameters (X-ray voltage = 55 kVp, Exposure time = 1100 ms and Pitch= 0.5). A total projection of 240 projects over 360° of rotation was acquired. Projected data were rebinned by 1:4 and reconstructed using a Ramlak filter.

Following the CT scans, animals were killed, perfused with PBS and tumours and muscle sections were removed and weighed. The radioactivities of each organ including tumours were measured using a gamma counter (Perkin Elmer). Tumour uptake was

then calculated as percentage injected dose/gram (% ID/g) of tumour over muscle signals.

In vivo Ultrasound Imaging

Ultrasound of animals was performed with a Vevo2100 small animal high frequency ultrasound scanner (VisualSonics Inc) using the MS250 non-linear contrast transducer. Animals were placed under light sedation (range of 1% to 2% isofluorane), on the VisualSonics imaging station. The imaging station was heated to prevent hypothermia. Imaging was performed on the flank of the animal where the tumour was induced. Animals were injected intravenously with either $scFv_{GPIIb/IIIa}$-MBs or $scFv_{mut}$-MBs.

Videos and images were acquired before, and at defined time points after injecting $1.5x10^7$ microbubbles in a total volume of 150 µL. Analysis was performed using VisualSonics imaging software (VisualSonics Inc).

Immunofluorescence of Cancer Cells and Platelets

Washed platelets were incubated with $5x10^5$ SkBr3 cells at 37°C for 2 hours. The platelets and cancer cell culture were then stained with CD41 (Beckman Coulter #A07781 or #IM0649U) and either PAC-1-FITC (BD Biosciences #340507), $scFv_{GPIIb/IIIa}$-GFP or CD62P (P-selectin) (BD Biosciences #550561) antibody for 30 min. Cells were fixed with BD Cytofix solution (BD Biosciences) and was imaged using the Nikon A1r Plus Confocal Microscope, 40x objective.

Immunohistochemistry of Human and Mouse Tumour Sections

Human tumour sections were obtained from biopsy specimens from patients with histologically confirmed breast, bowel or lung adenocarcinoma. Mouse of human tumour sections were fixed in formalin solution (Sigma Aldrich #HT501128) for 24 hours, paraffin embedded and microtome sectioned (Leica) to 5 µM – 30 µM onto a glass slide. Sections were deparaffinized, and underwent antigen retrieval with 0.01 M Citric Acid in 90°C for 20 min. Tumour sections were stained overnight with a polyclonal rabbit anti-CD41 antibody (Abcam #ab63983), and detected with an Alexa Fluor 647 labeled anti-rabbit antibody (Life Technologies #A-21245), counterstained with Hoechst® (Thermo Fisher Scientific #33342) and visualized using the Nikon A1r Plus Confocal Microscope, 60x oil objective.

Flow Cytometry of Tumour Cells

Tumours were excised from mice and placed into RPMI media. Ramos tumours and spleen sections were teased apart and filtered through a 100 µm filter into single cell suspensions. MDA-MB-231 tumours and mouse muscle sections were smashed in between two frosted slide glasses, digested with Liberase (Sigma #5401020001) for 2 hours and filtered through a 100 µm filter into single cell suspensions. Cells were then stained with mouse CD41 APC (eBioscience #17-0411) and flow cytometry was performed using a FACSCantoII scanner (BD Biosciences). Results were analyzed using the Flowlogic software.

Statistical Analysis

All data are reported as mean ± SEM of at least 3 independent assays unless otherwise noted. Statistical analyses were performed using unpaired Student's T tests for comparison of two groups and one way ANOVA for comparisons of more than two groups. A P value of less than 0.05 was considered significant.

Abbreviations

scFv: single chain antibodies; TXA_2: thromboxane-A_2; ADP: adenosine diphosphate; MMP-2: matrix metalloproteinase-2; PET: Positron Emission Tomography; CT: Computed Tomography; FLECT: Fluorescence Emission Computed Tomography; GPIIb/IIIa: Glycoprotein IIb/IIIa; IVIS: In vivo imaging system; ^{64}Cu: Copper-64; Mut: Mutant; BCN: bicyclo-[6.1.0]-non-4-yne; MB: Microbubbles; Cy7: Cyanine 7; ID/g: Injected dose per gram.

Acknowledgements

We thank Iśka Carmichael from the Monash Micro Imaging team for her technical support and the Monash Biomedical Imaging for access to the PET/CT and FLECT used for small animal imaging. Copper-64 was purchased and obtained from Stan Poniger and Henri Tochon-Danguy from the Centre for P.E.T. – Austin Health, Melbourne, Australia.

Funding

This work was funded by the National Health and Medical Research Council (NHMRC project grant: 1108670) of Australia. In addition, MLY is supported by the Australian Postgraduate Award Scholarship, JDM is supported by the Haematology Society of Australia and New Zealand (HSANZ) New Investigator Scholarship, XW is supported by the National Heart Foundation of Australia Postdoctoral Fellowship, PSD is supported by a Future Fellowship from the Australian Research Council, PMH is supported by the Rebecca Cooper Foundation and NHMRC project grants and KP is supported by an NHMRC Principal Research Fellowship.

Author contributions

MLY, JDM, XW, NAZ, JDH, MZ, YY, AP and BL designed and performed the experiments. MLY, JDM, XW, NAZ, JDH, MZ, YY, AP, MH, PSD, PMH, GAP, BL and KP analyzed the data. MLY, JDM, XW, GAP, MH, PSD, PMH, and KP wrote the manuscript. PSD and KP developed the technologies. PMH, GAP, BL and KP supervised the project. KP designed and conceived the project.

Competing Interests

KP is inventor on patents describing activated platelet-targeting recombinant antibodies. PSD is inventor on patents describing sarcophagine chelators for PET. All other authors have declared that no conflict of interest exists.

References

1. Siegel RL, Miller KD, Jemal A. Cancer statistics, 2016. *CA: A Cancer Journal for Clinicians*. 2016;66:7–30.
2. Rahib L, Smith BD, Aizenberg R, Rosenzweig AB, Fleshman JM, Matrisian LM. Projecting Cancer Incidence and Deaths to 2030: The Unexpected Burden of Thyroid, Liver, and Pancreas Cancers in the United States. *Cancer Res*. 2014;74:2913–2921.
3. Levin J, Conley CL. Thrombocytosis associated with malignant disease. *Arch Intern Med*. 1964;114:497–500.
4. Sierko E, Wojtukiewicz MZ. Platelets and angiogenesis in malignancy. *Semin Thromb Hemost*. 2004;30:95–108.
5. Jurasz P, Alonso-Escolano D, Radomski MW. Platelet–cancer interactions: mechanisms and pharmacology of tumour cell-induced platelet aggregation. *Br J Pharmacol*. 2004;143:819–826.
6. Gasic GJ, Gasic TB, Stewart CC. Antimetastatic effects associated with platelet reduction. *Proc Natl Acad Sci U S A*. 1968;61:46–52.
7. Bastida E, Escolar G, Ordinas A, Jamieson GA. Morphometric evaluation of thrombogenesis by microvesicles from human tumor cell lines with thrombin-dependent (U87MG) and adenosine diphosphate-dependent (SKNMC) platelet-activating mechanisms. *J Lab Clin Med*. 1986;108:622–627.
8. Alonso-Escolano D, Strongin AY, Chung AW, Deryugina EI, Radomski MW. Membrane type-1 matrix metalloproteinase stimulates tumour cell-induced platelet aggregation: role of receptor glycoproteins. *British Journal of Pharmacology*. 2004;141:241–252.
9. Medina C, Jurasz P, Santos-Martinez MJ, Jeong SS, Mitsky T, Chen R, Radomski MW. Platelet Aggregation-Induced by Caco-2 Cells: Regulation by Matrix Metalloproteinase-2 and Adenosine Diphosphate. *J Pharmacol Exp Ther*. 2006;317:739–745.
10. Karpatkin S, Pearlstein E, Ambrogio C, Coller BS. Role of adhesive proteins in platelet tumor interaction in vitro and metastasis formation in vivo. *J Clin Invest*. 1988;81:1012–1019.
11. Chopra H, Hatfield JS, Chang YS, Grossi IM, Fitzgerald LA, O'Gara CY, Marnett LJ, Diglio CA, Taylor JD, Honn KV. Role of tumor cytoskeleton and membrane glycoprotein IRGpIIb/IIIa in platelet adhesion to tumor cell membrane and tumor cell-induced platelet aggregation. *Cancer Res*. 1988;48:3787–3800.
12. Oleksowicz L, Dutcher JP. Adhesive receptors expressed by tumor cells and platelets: novel targets for therapeutic anti-metastatic strategies. *Med Oncol*. 1995;12:95–102.
13. Stone JP, Wagner DD. P-selectin mediates adhesion of platelets to neuroblastoma and small cell lung cancer. *Journal of Clinical Investigation*. 1993;92:804.
14. Bennett JS. Structure and function of the platelet integrin αIIbβ3. *J Clin Invest*. 2005;115:3363–3369.
15. Ma Y-Q, Qin J, Plow EF. Platelet integrin αIIbβ3: activation mechanisms. *Journal of Thrombosis and Haemostasis*. 2007;5:1345–1352.
16. Schwarz M, Meade G, Stoll P, Ylanne J, Bassler N, Chen YC, Hagemeyer CE, Ahrens I, Moran N, Kenny D, Fitzgerald D, Bode C, Peter K. Conformation-Specific Blockade of the Integrin GPIIb/IIIa A Novel Antiplatelet Strategy That Selectively Targets Activated Platelets. *Circulation Research*. 2006;99:25–33.
17. Stoll P, Bassler N, Hagemeyer CE, Eisenhardt SU, Chen YC, Schmidt R, Schwarz M, Ahrens I, Katagiri Y, Pannen B, Bode C, Peter K. Targeting Ligand-Induced Binding Sites on GPIIb/IIIa via Single-Chain Antibody Allows Effective Anticoagulation Without Bleeding Time Prolongation. *Arteriosclerosis, Thrombosis, and Vascular Biology*. 2007;27:1206–1212.
18. Schwarz M, Röttgen P, Takada Y, Le Gall F, Knackmuss S, Bassler N, Büttner C, Little M, Bode C, Peter K. Single-chain antibodies for the conformation-specific blockade of activated platelet integrin alphaIIbbeta3 designed by subtractive selection from naive human phage libraries. *FASEB J*. 2004;18:1704–1706.
19. Phillips DR, Charo IF, Parise LV, Fitzgerald LA. The platelet membrane glycoprotein IIb-IIIa complex. *Blood*. 1988;71:831–843.
20. Armstrong PC, Peter K. GPIIb/IIIa inhibitors: from bench to bedside and back to bench again. *Thromb Haemost*. 2012;107:808–814.
21. Alt K, Paterson BM, Ardipradja K, Schieber C, Buncic G, Lim B, Poniger SS, Jakoby B, Wang X, O'Keefe GJ, Tochon-Danguy HJ, Scott AM, Ackermann U, Peter K, Donnelly PS, Hagemeyer CE. Single-Chain Antibody Conjugated to a Cage Amine Chelator and Labeled with Positron-Emitting Copper-64 for Diagnostic Imaging of Activated Platelets. *Mol Pharmaceutics*. 2014;11:2855–2863.
22. Paterson BM, Roselt P, Denoyer D, Cullinane C, Binns D, Noonan W, Jeffery CM, Price RI, White JM, Hicks RJ, Donnelly PS. PET imaging of tumours with a 64Cu labeled macrobicyclic cage amine ligand tethered to Tyr3-octreotate. *Dalton Trans*. 2013;43:1386–1396.
23. Wang X, Hagemeyer CE, Hohmann JD, Leitner E, Armstrong PC, Jia F, Olschewski M, Needles A, Peter K, Ahrens I. Novel Single-Chain Antibody-Targeted Microbubbles for Molecular Ultrasound Imaging of Thrombosis Validation of a Unique Noninvasive Method for Rapid and Sensitive Detection of Thrombi and Monitoring of Success or Failure of Thrombolysis in Mice. *Circulation*. 2012;125:3117–3126.
24. Lim B, Yao Y, Huang AL, Yap ML, Flierl U, Palasubramaniam J, Zaldivia MTK, Wang X, Peter K. A Unique Recombinant Fluoroprobe Targeting Activated Platelets Allows *In Vivo* Detection of Arterial Thrombosis and Pulmonary Embolism Using a Novel Three-Dimensional Fluorescence Emission Computed Tomography (FLECT) Technology. *Theranostics*. 2017;7:1047–1061.
25. Wang X, Hagemeyer CE, Hohmann JD, Leitner E, Armstrong PC, Jia F, Olschewski M, Needles A, Peter K, Ahrens I. Novel Single-Chain Antibody-Targeted Microbubbles for Molecular Ultrasound Imaging of Thrombosis Validation of a Unique Noninvasive Method for Rapid and Sensitive Detection of Thrombi and Monitoring of Success or Failure of Thrombolysis in Mice. *Circulation*. 2012;125:3117–3126.
26. Ziegler M, Alt K, Paterson BM, Kanellakis P, Bobik A, Donnelly PS, Hagemeyer CE, Peter K. Highly Sensitive Detection of Minimal Cardiac Ischemia using Positron Emission Tomography Imaging of Activated Platelets. *Scientific Reports*. 2016;6:38161.
27. Elverfeldt D von, Maier A, Duerschmied D, Braig M, Witsch T, Wang X, Mauler M, Neudorfer I, Menza M, Idzko M, Zirlik A, Heidt T, Bronsert P, Bode C, Peter K, Muhlen C von zur. Dual-Contrast Molecular Imaging Allows Noninvasive Characterization of Myocardial Ischemia/Reperfusion Injury After Coronary Vessel Occlusion in Mice by Magnetic Resonance ImagingCLINICAL PERSPECTIVE. *Circulation*. 2014;130:676–687.
28. Wang X, Gkanatsas Y, Palasubramaniam J, Hohmann JD, Chen YC, Lim B, Hagemeyer CE, Peter K. Thrombus-Targeted Theranostic Microbubbles: A New Technology towards Concurrent Rapid Ultrasound Diagnosis and Bleeding-free Fibrinolytic Treatment of Thrombosis. *Theranostics*. 2016;6:726–738.
29. Hohmann JD, Wang X, Krajewski S, Selan C, Haller CA, Straub A, Chaikof EL, Nandurkar HH, Hagemeyer CE, Peter K. Delayed targeting of CD39 to activated platelet GPIIb/IIIa via a single-chain antibody: breaking the link between antithrombotic potency and bleeding? *Blood*. 2013;121:3067–3075.
30. Kim W, Haller C, Dai E, Wang X, Hagemeyer CE, Liu DR, Peter K, Chaikof EL. Targeted antithrombotic protein micelles. *Angew Chem Int Ed Engl*. 2015;54:1461–1465.
31. Hagemeyer CE, Alt K, Johnston APR, Such GK, Ta HT, Leung MKM, Prabhu S, Wang X, Caruso F, Peter K. Particle generation, functionalization and sortase A–mediated modification with targeting of single-chain antibodies for diagnostic and therapeutic use. *Nat Protocols*. 2015;10:90–105.